Available online at www.sciencedirect.com
ScienceDirect
Journal of the European Ceramic Society 26 (2006) 3399–3405
www.elsevier.com/locate/jeurceramsoc

Reinforcement of precursor-derived Si–C–N ceramics with carbon nanotubes

Yuji Katsuda [a,b,*], Peter Gerstel [a], Janakiraman Narayanan [a], Joachim Bill [a,**], Fritz Aldinger [a]

[a] *Max-Planck-Institut für Metallforschung and Institut für Nichtmetallische Anorganische Materialien, Universität Stuttgart, Pulvermetallurgisches Laboratorium, Heisenbergstr. 3, D-70569 Stuttgart, Germany*
[b] *Materials Research Laboratory, NGK Insulators Ltd., 2-56 Suda-cho, Mizuho, 467-8530 Nagoya, Japan*

Received 28 May 2005; received in revised form 11 October 2005; accepted 17 October 2005
Available online 19 December 2005

Abstract

Nanocomposites consisting of precursor-derived Si–C–N ceramics incorporated with carbon nanotubes (CNTs) were successfully prepared by casting of a mixture of CNTs and a liquid precursor polymer followed by cross-linking and thermolysis. The effect of CNTs on the fracture toughness of these nanocomposites was investigated by a thermal loading technique. The results reveal a dependence of the fracture toughness on the type of the CNTs. One type shows a significant increase of the fracture toughness at CNT contents of only 1–2 mass%, whereas the other one exhibits no effect. The microstructural effects of CNTs observed at the fracture surfaces of the nanocomposites by scanning electron microscope (SEM) and transmission electron microscope (TEM) can be correlated with the observed fracture toughness behavior.

Keywords: Nanocomposites; Toughness and toughening; Electron microscopy; Precursors-organic; Carbon nanotubes

1. Introduction

CNTs are seamless cylinders of graphene sheets either in the form of single-walled (SW) or multi-walled (MW) assemblies. Much research has been dedicated to the understanding of CNTs revealing their superior properties. For example, SWCNTs are known to have a Young's modulus of above 1 TPa,[1,2] tensile strength of above 30 GPa,[2] thermal conductivity at room temperature up to 6600 W/mK[3,4] and metallic or semiconductive behavior depending on the helicity of the graphene sheets.[5–7] CNTs are expected to be used, e.g. for the production of such electric devices as field emission displays,[8] nanometer-sized semiconductors,[9] supercapacitors for energy storage[10] or filler materials to induce or improve the electrical, thermal or mechanical functions.[11–15] Especially from the mechanical viewpoint, CNTs are promising reinforcement materials combining a low weight, nanometer size and a high aspect ratio (length to radius).

In the case of polymer matrix CNT composites, the mixing process with liquid polymers enables CNTs to be highly dispersed and the following low heat-treatment temperature excludes the destruction of CNTs during the matrix densification. Sandler et al.[11] studied the electrical conductivity of epoxy matrix CNT composites and determined the percolation threshold to be below 0.04 vol.%. Gojny et al.[13] investigated the mechanical properties of similar composites and revealed a fracture toughness increase by ca. 25% with the incorporation of 1 vol.% double-walled CNTs.

Concerning the ceramic-matrix CNT composites, conventional powder technological techniques including powder mixing and high temperature sintering might cause CNTs to lose their integrity which is necessary to fulfil their function in the matrix. Because of that, Zahn et al.[15] demonstrated the effectiveness of spark plasma sintering for the preparation of alumina matrix CNT composites, where a significant increase in the fracture toughness was obtained with 10 vol.% of SWCNT incorporation. It was concluded that the low sintering temperature and short duration might give less damage on CNTs during alumina sintering.

* Corresponding author. Tel.: +81 52 872 7895; fax: +81 52 872 7537.
** Corresponding author. Tel.: +49 711 689 3228; fax: +49 711 689 3131.
E-mail addresses: katsuda@ngk.co.jp (Y. Katsuda), bill@mf.mpg.de (J. Bill).

0955-2219/$ – see front matter © 2005 Elsevier Ltd. All rights reserved.
doi:10.1016/j.jeurceramsoc.2005.10.014

Ternary Si–C–N ceramics can be obtained by thermolysis of organometallic precursor polymers at relatively low temperatures.[16,17] They are predominantly amorphous or nanocrystalline materials and possess excellent structural stability leading to high creep and corrosion resistance at high temperatures.[18,19] One of the distinctive process features of precursor-derived ceramics is the unique polymer-ceramic transformation by heat treatment, which can provide a means to form ceramic bodies into near-net shapes, small scales or complex forms from cross-linked polymer bodies. In this connection, Raj[20] applied precursor-derived Si–C–N ceramics to microelectromechanical devices (MEMS technologies).

However, a main drawback of precursor-derived ceramics is their brittle nature leading to a deterioration of their mechanical properties. The incorporation of toughening agents to form composites is an approach to reinforce the brittle ceramics. From this point of view, An et al.[21] recently synthesized MWCNT-reinforced Si–C–N ceramics by catalytic cross-linking and pressure assisted pyrolysis from mixtures of a precursor and CNTs. They revealed a Young's modulus, hardness and damage resistance increase with 6.4 vol.% MWCNT incorporation into Si–C–N ceramics. However, the effect on the fracture toughness behavior is still unclear.

This paper describes the incorporation of MWCNTs into polymer-derived Si–C–N ceramics applying a casting process followed by pressureless cross-linking and thermolysis. The effect of MWCNTs on the fracture toughness behavior of nanocomposites is investigated by a thermal loading technique, where the crack propagation induced by thermal stress is analyzed. The results are mainly discussed in connection with microstructural features characterized by scanning electron (SEM) and transmission electron microscopy (TEM). Two types of MWCNTs are used to compare and differentiate the effect of reinforcement.

2. Experimental

A commercial liquid polyureasilazane (Ceraset, KION, USA) was used as the starting precursor polymer for Si–C–N ceramics. Two types of MWCNTs (type A: NanoLab, USA, Lot.: 091002LPG and type B: Nanocs Inc., USA) were applied for the reinforcements. In typical experiment, the CNTs (30–70 mg) were dispersed in tetrahydrofuran (30 ml) as a solvent and deagglomerated by direct sonication for 1 h using a probe type ultrasonic generator (SONOPULS HD2200, BANDELIN Electronic, Germany). The liquid polysilazane (5 g) was then added into the suspension and mixed by stirring. After the removal of tetrahydrofuran in vacuum under stirring, the obtained viscous mixture of CNTs and polyureasilazane was cast into a Teflon mold (18 mm in diameter and 1 mm in thickness) in a metal die and heat-treated at 360 °C for 6 h in an argon atmosphere to cross-link and solidify the precursor polymer. Finally, the solidified bodies were thermolysed at 1000 °C for 1 h in an argon atmosphere (heating rate of 25 °C/h). The contents of CNTs in the Si–C–N nanocomposites were adjusted from 0 to 2 in mass%, which corresponds approximately to the volume content (vol.%).[22]

The density and thermal expansion of the prepared materials were characterized by conventional techniques using Archimedes' principle and a push rod dilatometer, respectively. The elastic properties were measured by a resonant frequency and damping analyzer (Integrated Material Control Engineering n.V., Belgium). Microstructural characterization was performed with a SEM (JSM-6300F, JEOL) and a TEM (CM200, Philips).

The thermal loading technique[23–25] with an edge-cracked circular disk (12 mm in diameter and 0.25 mm in thickness) was used to determine the fracture toughness behavior of the nanocomposites. In this technique, the thermal stress is induced into the specimen by irradiation with a tungsten lamp (150 W), where the rate of applied voltage (1 V/130 s) is precisely controlled to produce the desired temperature distribution in the specimen. The stress intensity factor K_I can be defined by the thermal stress field $\sigma(x)$ and the Weight function parameter $h(x, a)$ in Eq. (1) developed by Brueckner[26];

$$K_I = \int_0^a h(x, a)\sigma(x)\mathrm{d}x, \tag{1}$$

where a is the crack length and x is the distance from the edge. For a single edge-cracked disk, the solution of $h(x, a)$ determined by Fett and Munz[27] in Eq. (2) can be applied;

$$h(x, a) = \sqrt{\frac{2}{\pi a}}\left[\frac{\rho}{\sqrt{1-\rho}} + D_0\sqrt{1-\rho} + D_1(1-\rho)^{3/2} + D_2(1-\rho)^{5/2}\right], \quad \rho = \frac{x}{a}, \tag{2}$$

where D_0, D_1 and D_2 are coefficient functions derived by the crack length (see the Appendix A).

The stress distribution $\sigma(r)$ produced in the tangential direction of a circular disk can be defined as Eq. (3)[28] by using a temperature distribution $T(r)$;

$$\sigma(r) = \alpha E\left[\frac{1}{R^2}\int_0^R T(r)r\mathrm{d}r + \frac{1}{r^2}\int_0^r T(r)r\mathrm{d}r - T(r)\right] \tag{3}$$

where x is converted to r by $x = R - r$, R is the radius of the disk, r is the radial distance from the center, α is the coefficient of thermal expansion and E is the Young's modulus. In the present study, the measured temperature distribution $T(r, t)$ could be reasonably fitted by a fourth order polynomial[23–25] as in Eq. (4);

$$T(r, t) = c_0(t) + c_2(t)r^2 + c_4(t)r^4 \tag{4}$$

where c_0, c_2 and c_4 are time-dependent fitting parameters and t is the time. Finally, the time- and crack-length-dependent stress intensity factor K_I as well as K_{Ic} at the crack tip can be calculated by using the crack length time relation monitored by a CCD camera and the measured α and E profiles.

3. Results and discussion

First, both MWCNTs (types A and B) were characterized by electron microscopy. The micrographs are shown in Figs. 1 and 2, respectively. From the SEM micrographs in Fig. 1, it can be seen that the type A-CNTs are smaller in diameter and

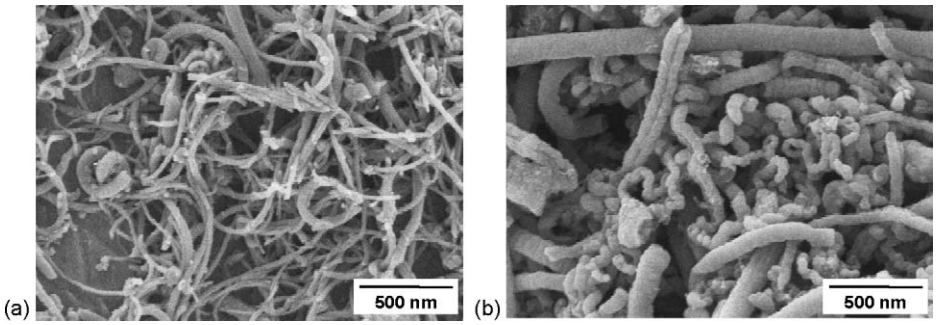

Fig. 1. SEM micrographs showing the morphology of MWCNTs: (a) type A, high aspect ratio and (b) type B, low aspect ratio.

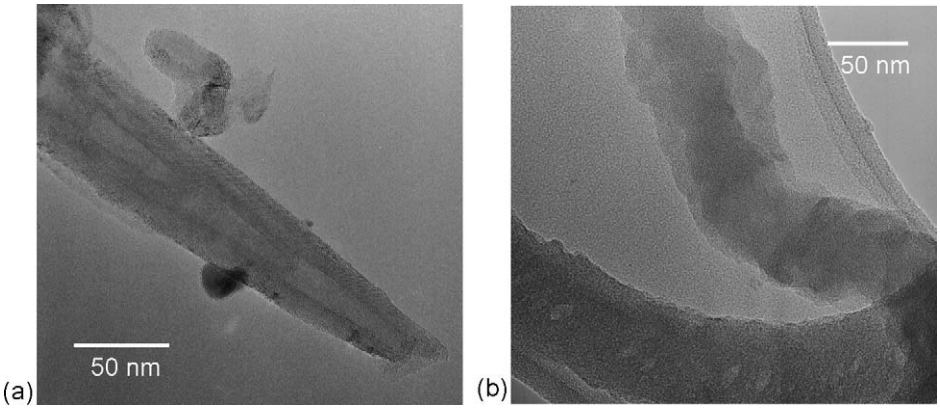

Fig. 2. TEM micrographs of MWCNTs: (a) type A, (b) type B.

relatively longer than the type B ones, which indicates that type A has a high aspect ratio (length to radius). The TEM micrographs in Fig. 2 reveal that type A-CNTs exhibited the characteristic hollow structure of CNTs with several stacked graphene sheets. In contrast, type B-CNTs show a stuffed structure inside with no distinctive graphene sheets indicating an amorphous nature in the majority.

The representative microstructures at fracture surfaces of cross-linked materials are shown in Fig. 3. The pure Si–C–N precursor (Fig. 3a) shows a featureless surface apart from some

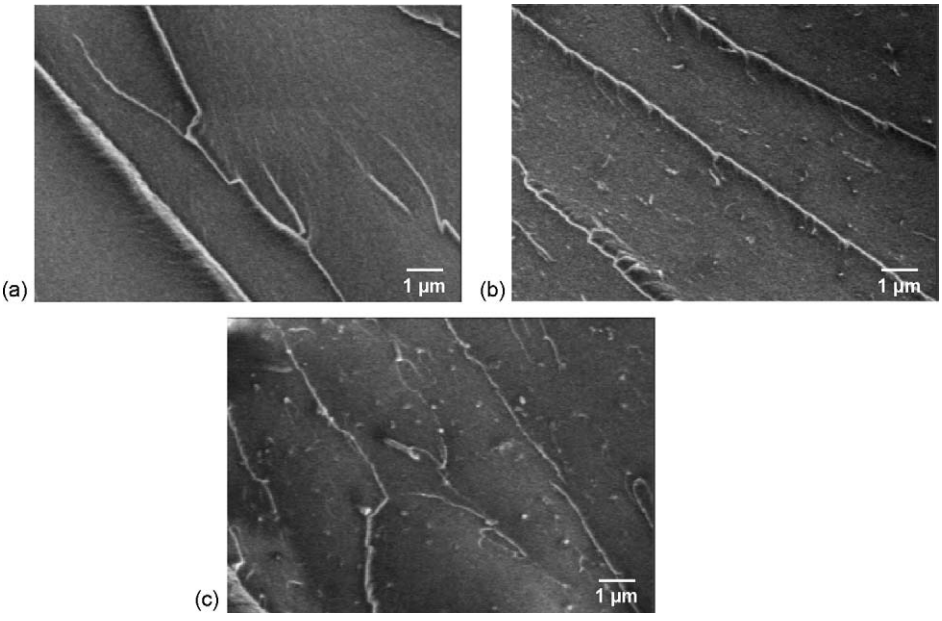

Fig. 3. SEM micrographs of the fracture surface of cross-linked bodies derived from the pure Si–C–N precursor (a), 2 mass% type A nanocomposite (b) and 2 mass% type B nanocomposite (c).

Table 1
Materials properties of Si–C–N ceramics incorporated with MWCNTs

CNT	Amount (mass%)	Bulk density (g/cm^3)	Young's modulus (GPa)	Poisson's ratio	CTE 50-800C (10^{-6}/K)
–	0	2.15	138	0.21	3.5
Type A	1	2.19	138	0.22	–
Type A	2	2.21	140	0.21	3.4
Type B	1	2.18	139	0.22	–
Type B	2	2.16	138	0.22	3.4

steps which arise from the cleavage of the material. In both cross-linked composites (Fig. 3b and c), CNTs are observed as pullout features uniformly distributed. In contrast to the fracture surface found within CNT-epoxy composites,[14] no holes at the interfaces between the CNTs and the cross-linked matrix are observed, indicating the strong bonding nature of CNTs to the cross-linked matrix.

The cross-linked materials were thermolysed at 1000 °C for 1 h in an argon atmosphere, where the linear shrinkage and weight loss during the thermolysis in all materials were ca. 25% and ca. 20%, respectively. The thermolysed materials exhibited an amorphous nature as revealed by XRD. Some of their materials properties are summarized in Table 1. It is confirmed that there are no significant differences in the bulk density, Young's modulus, Poisson's ratio and coefficient of thermal expansion (CTE) among the materials prepared in this study. That is, the addition of CNTs up to 2 mass% does not influence the basic material properties of the nanocomposites.

Fig. 4 shows the measured temperature distribution in the pure Si–C–N ceramic produced by a lamp heating (closed circles) and the fitted profiles by a fourth order polynomial as in Eq. (4) (solid lines) for different lamp voltages. The representative fracture toughness behavior of nanocomposites as a function of crack length measured by this thermal loading technique is

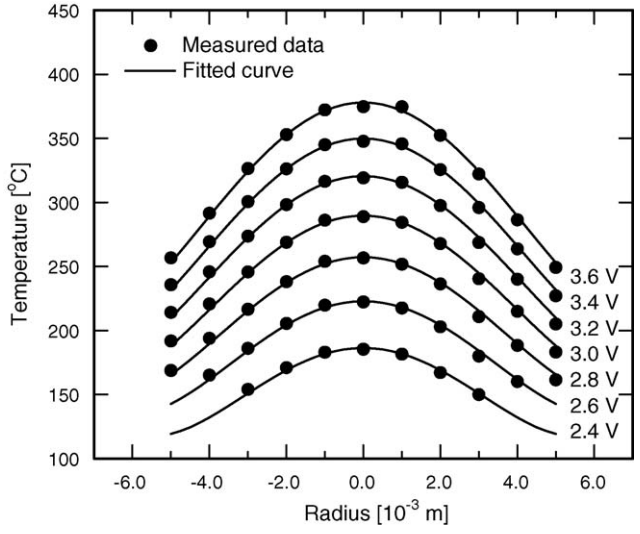

Fig. 4. Temperature distribution of the pure Si–C–N ceramic produced by a lamp heating, measured data (closed circles) and the fitted profiles (solid lines) for different lamp voltages (radius = 0 represents the center of the disc-shaped specimen).

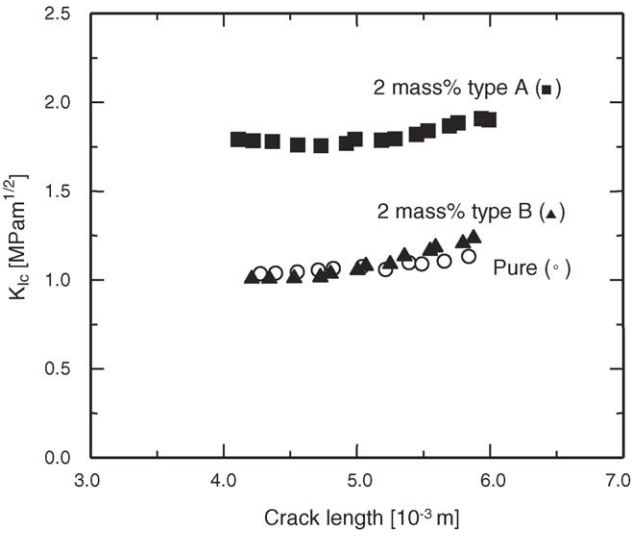

Fig. 5. Fracture toughness behavior of Si–C–N nanocomposites as a function of the crack length.

shown in Fig. 5. It reveals that each material shows nearly constant fracture toughness during crack propagation but that the magnitudes are much different among the considered materials. The averaged fracture toughness values are plotted in Fig. 6 as a function of the CNT content. As can be seen from the diagram, the incorporation of type A-CNT significantly increases the fracture toughness of Si–C–N ceramics even at content as low as 1 mass%. With a content of 2 mass%, the increase of K_{Ic} reaches more than 60% as compared to the pure Si–C–N material. On the other hand, the addition of type B-CNTs has no effect on the fracture toughness as revealed by behavior similar to that of the pure material.

Typical microstructures at the crack faces of 2 mass% CNT nanocomposites after fracture toughness measurement are shown in Fig. 7. There exists a big difference between the two types of nanocomposites, where CNTs lead to pullout and

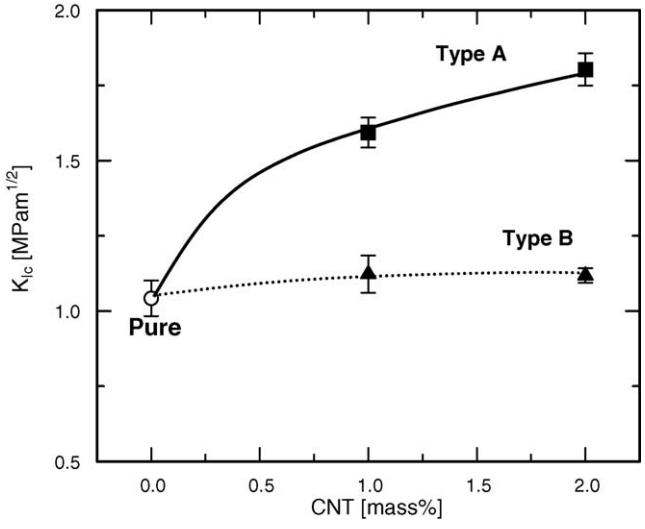

Fig. 6. Fracture toughness behavior of Si–C–N nanocomposites as a function of the CNT content.

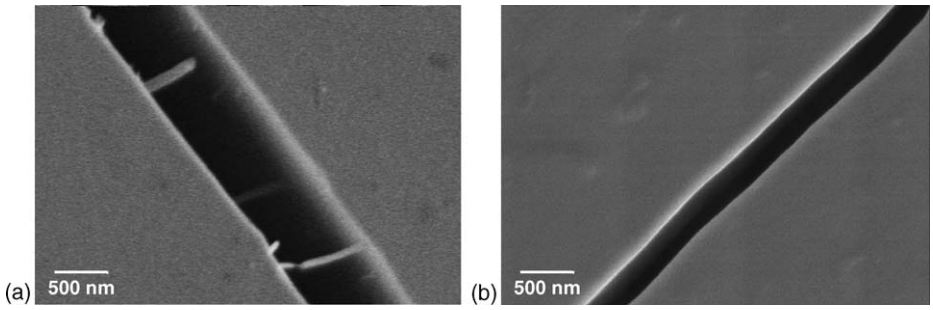

Fig. 7. SEM micrographs at the crack face of Si–C–N nanocomposites after fracture toughness measurement. Both (a) type A and (b) type B contain 2 mass% of CNTs in the matrix.

bridging structures in the type A nanocomposite, whereas no CNTs are observed in the other one in a way similar to the pure Si–C–N material. Further SEM investigations were performed on matching fracture faces created during fracture toughness measurement (Fig. 8). The pure Si–C–N (Fig. 8a) shows only a flat featureless structure in accordance with the amorphous nature of the materials. In the type A nanocomposites (Fig. 8b and c), besides some CNTs pulled out from the matrix (marked X), the corresponding holes (marked X′) are also observed at the opposite face. Furthermore, a few broken CNTs can be determined (Y and Y′) in pairs at both surface levels. That is, two CNT features of pulled out and broken are identified on the fracture surface of the type A-CNT nanocomposites. On the other hand in the case of the other nanocomposite (Fig. 8d and e), only highly distributed dark parts from the traces of CNTs are observed instead of pulled out or broken CNTs, indicating a deterioration of the CNTs structure in the matrix during thermolysis.

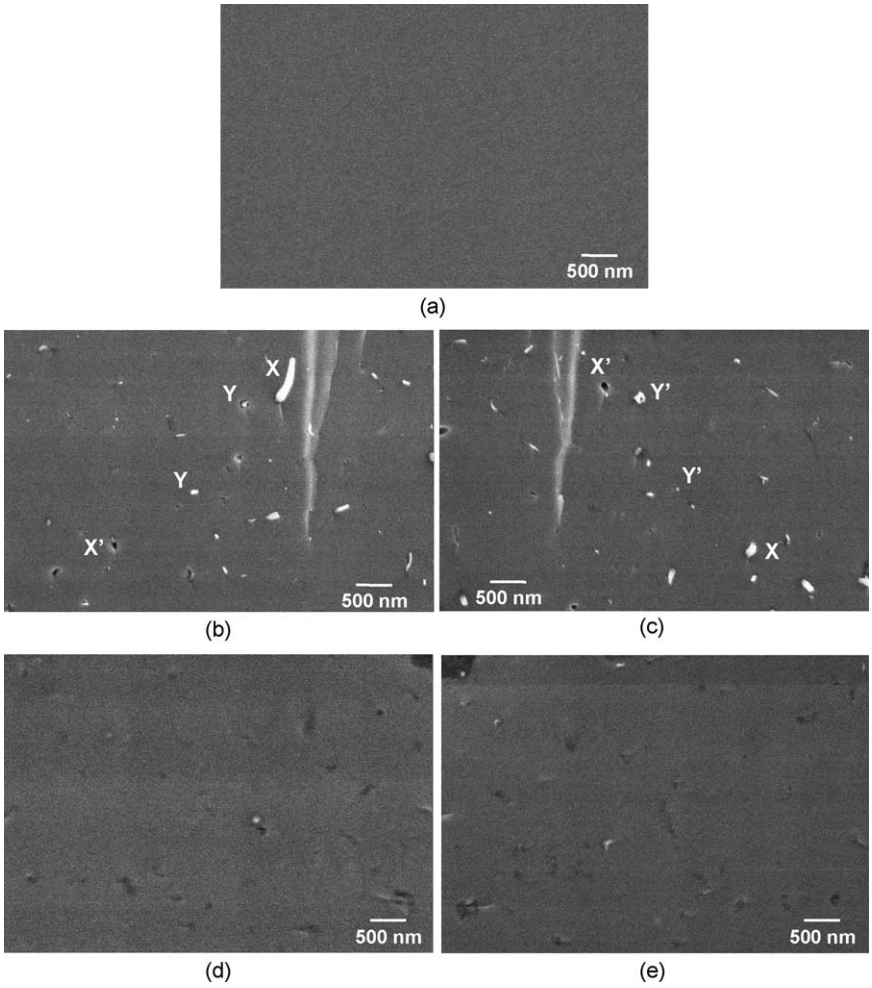

Fig. 8. SEM micrographs of the matching fracture faces of Si–C–N nanocomposites after fracture toughness measurement: (a) pure Si–C–N ceramic, (b and c) 2 mass% type A and (d and e) 2 mass% type B nanocomposite. The notes X–X′ and Y–Y′ indicate pullout CNT-hole and broken CNT pair structure, respectively.

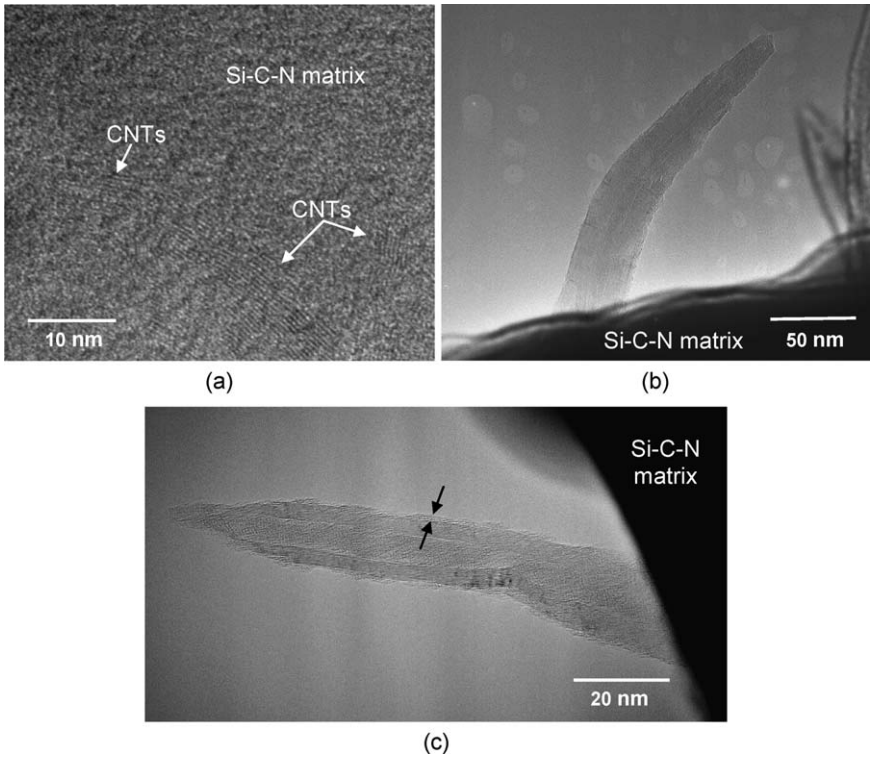

Fig. 9. TEM micrographs of 2 mass% CNTs (type A) Si–C–N nanocomposites: (a) embedded CNTs in the Si–C–N matrix, where white arrows indicate CNTs and their boundary to the matrix; (b and c) CNTs pulled out from the matrix after fracture toughness measurement, where a bare CNT (b) and a broken CNT covered with the matrix (c) are shown. Black arrows in (c) indicate the matrix layer attached to the pulled out CNT.

TEM micrographs of Si–C–N nanocomposites incorporated with type A-CNT (2 mass%) are shown in Fig. 9. The embedded CNTs in the matrix (Fig. 9a) of an ion-thinned sample clearly reveal their multi-walled structure as in the initial state indicating the preservation of their mechanical nature in the nanocomposites. Moreover, no crevices can be observed at the interface between CNTs and the matrix revealing the existence of the well-bonded nature at their interfaces. Within pulled out CNTs after fracture toughness measurement, two types of CNT features consisting of bare CNTs (Fig. 9b) and broken CNTs covered with the matrix layer (Fig. 9c) were observed. These different features are in accordance with the high strength of the embedded CNTs in combination with the well-balanced interface between CNTs and the matrix, as revealed by the presence of both pulled out and broken nanotubes.

Consequently, the increase of the fracture toughness is considered to be due to the tensile load carrying of type A-CNTs via the interfacial bonding between CNTs and the Si–C–N matrix. On the other hand in type B nanocomposites, the existence of CNTs and their boundary could not be clearly identified by TEM or SEM analysis indicating a degeneration of the CNTs in the matrix during thermolysis. This may be trace back to the amorphous nature of type B-CNTs, which reveals the importance of the CNTs nature for reinforcement.

4. Summary

Two types of MWCNTs have been incorporated into the Si–C–N ceramics via casting of a mixture of CNTs and a precursor polymer followed by pressureless cross-linking and thermolysis. The mechanical studies by a thermal loading technique reveal remarkable increase in the fracture toughness of the nanocomposites, where pulling out, bridging up and breaking of CNTs are observed at the fracture surfaces. The TEM analyses demonstrate the preservation of MWCNTs structure in the Si–C–N matrix and the existence of the well-bonded interface between CNTs and the Si–C–N matrix. On the other hand, the CNTs possessing an amorphous nature provide no effect on the mechanical properties of the nanocomposites.

Acknowledgements

The authors thank Prof. R. Danzer, University of Leoben, Austria and Prof. R. Raj, University of Colorado, USA for helpful discussions. Mr. R. Mager, Ms. S. Kühnemann and Ms. M. Kelsch, Max-Planck-Institut für Metallforschung, are gratefully acknowledged for their technical support.

Appendix A

$$D_0 = \frac{1.5721 + 2.4109\beta - 0.8968\beta^2 - 1.4311\beta^3}{(1-\beta)^{3/2}}$$

$$D_1 = \frac{0.4621 + 0.5972\beta + 0.7466\beta^2 + 2.2131\beta^3}{(1-\beta)^{3/2}}$$

$$D_2 = \frac{-0.2537 + 0.4353\beta - 0.2851\beta^2 - 0.5853\beta^3}{(1-\beta)^{3/2}}$$

$$\beta = \frac{a}{2R}$$

References

1. Krishnan, A., Dujardin, E., Ebbesen, T. W., Yianilos, P. N. and Treacy, M. M. J., Young's modulus of single-walled nanotubes. *Phys. Rev. B*, 1998, **58**, 14013–14019.
2. Yu, M.-F., Files, B. S., Arepalli, S. and Ruoff, R. S., Tensile loading of ropes of single wall carbon nanotubes & their mechanical properties. *Phys. Rev. Lett.*, 2000, **84**, 5552–5555.
3. Hone, J., Whitney, M. and Zettl, A., Thermal conductivity of single-walled carbon nanotubes. *Synth. Metals*, 1999, **103**, 2498–2499.
4. Berber, S., Kwon, Y.-K. and Tomanek, D., Unusually high thermal conductivity of carbon nanotubes. *Phys. Rev. Lett.*, 2000, **84**, 4613–4616.
5. Mintmire, J. W., Dunlap, B. I. and White, C. T., Are fullerene tubules metallic? *Phys. Rev. Lett.*, 1992, **68**, 631–6341.
6. Hamada, N., Sawada, S. and Oshima, A., New one-dimensional conductors: Graphite microtubules. *Phys. Rev. Lett.*, 1992, **68**, 1579–1581.
7. Saito, R., Fujita, M., Dresselhaus, G. and Dresselhaus, M. S., Electric structure of chiral graphene tubules. *Appl. Phys. Lett.*, 1992, **60**, 2204–22061.
8. Choi, W. B., Chung, D. S., Kang, J. H., Kim, H. Y., Jin, Y. W., Han, I. T. *et al.*, Fully sealed, high-brightness carbon-nanotube field-emission display. *Appl. Phys. Lett.*, 1999, **75**, 3129–3131.
9. Graham, A. P., Duesberg, G. S., Seidel, R., Liebau, M., Unger, E., Kreupl, F. *et al.*, Towards the integration of carbon nanotubes in microelectronics. *Diamond Relat. Mater.*, 2004, **13**, 1296–1300.
10. Emmenegger, Ch., Mauron, Ph., Sudan, P., Wenger, P., Hermann, V., Gallay, R. *et al.*, Investigation of electochamical double-layer (ECDL) capacitors electrodes based on carbon nanotubes & activated carbon materials. *J. Power Sources*, 2003, **124**, 321–329.
11. Sandler, J. K. W., Kirk, J. E., Kinloch, I. A., Shaffer, M. S. P. and Windle, A. H., Ultra-low electrical percolation threshold in carbon-nanotube-epoxy composites. *Polymer*, 2003, **44**, 5893–5899.
12. Biercuk, M. J., Llaguno, M. C., Radosavljevic, M., Hyun, J. K. and Johnson, A. T., Carbon nanotubecomposites for thermal management. *Appl. Phys. Lett.*, 2002, **80**, 2767–2769.
13. Gojny, F. H., Wichmann, M. H. G., Koepke, U., Fieldler, B. and Schulte, K., Carbon nanotubes-reinforced epoxy-composites: enhanced stiffness & fracture toughness at low nanotubes content. *Compos. Sci. Technol.*, 2004, **64**, 2363–2371.
14. Lau, K. T. and Hui, D., Effectiveness of using carbon nanotubes as nano-reinforcements for advanced composite structures. *Carbon*, 2002, **40**, 1597–1617.
15. Zhan, G. D., Kuntz, J. D., Wan, J. and Mukherjee, A. K., Single-wall carbon nanotubes as attractive toughening agents in alumina-based nanocomposites. *Nat. Mater.*, 2003, **2**, 38–42.
16. Bill, J. and Aldinger, F., Precursor-derived cova1ent ceramics. *Adv. Mater.*, 1995, **7**, 775–787.
17. Bill, J., Kamphowe, T. W., Mueller, A., Wichmann, T., Zern, A., Jalowieki, A. *et al.*, Precursor-derived Si-(B-)C-N ceramics: thermolysis, amorphous state & crystallization. *Appl. Organomet. Chem.*, 2001, **15**, 777–793.
18. Thurn, G., Canel, J., Bill, J. and Aldinger, F., Compression creep behaviour of precursor-derived Si–C–N ceramics. *J. Eur. Ceram. Soc.*, 1999, **19**, 2317–2323.
19. Raj, R., An, L. and Shah, S., Oxidation kinetics of an amorphous silicon carbonitride ceramics. *J. Am. Ceram. Soc.*, 2001, **84**, 1803–1810.
20. Raj, R., Ceramic MEMS. New materials, innovative processing & future applications. *Am. Ceram. Soc. Bull.*, 2001, **80**, 25–30.
21. An, L., Xu, W., Rajagopalan, S., Wang, C., Wang, H., Fan, Y. *et al.*, Carbon-nanotube-reinforced polymer-derived ceramic composites. *Adv. Mater.*, 2004, **16**, 2036–2040.
22. Lu, J. P. and Han, J., Carbon nanotubes and nanotubes-based nano devices. *Int. J. High Speed Electron. Sys.*, 1998, **9**, 101–123.
23. Schneider, G. A. and Petzow, G., Thermal shock testing of ceramics-A new testing method. *J. Am. Ceram. Soc.*, 1991, **74**, 98–102.
24. Margerl, F., Schneider, G. A. and Petzow, G., Crack initiation and crack growth in ceramics under thermal loading. *Adv. Mater.*, 1993, 395–399. I/A: Ceramics, powders, corrosion and advanced processing.
25. Schneider, G. A. and Danzer, R., Calculation of the stress intensity factor of an edge crack in a finite elastic disc using the weight function method. *Fract. Mech.*, 1989, **34**, 547–552.
26. Brueckner, H., A novel principle for the computation of stress intensity factors. *ZAMM*, 1970, **50**, 529–546.
27. Fett, T. and Munz, D., *Stress Intensity Factors and Weight Functions*. Computational Mechanics Publications, Southampton, 1997, pp. 149–153.
28. Boley, B. A. and Weiner, J. H., *Theory of Thermal Stresses*. R.E. Krieger, Malabar, FL, 1985, pp. 288–291.